



# VisionTS++: Cross-Modal Time Series Foundation Model with Continual Pre-trained Visual Backbones

Lefei Shen<sup>1,\*</sup>, Mouxiang Chen<sup>1,\*</sup>, Xu Liu<sup>2</sup>, Han Fu<sup>1</sup>,  
 Xiaoxue Ren<sup>1</sup>, Jianling Sun<sup>1</sup>, Zhuo Li<sup>3,†</sup>, Chenghao Liu<sup>4,†</sup>

<sup>1</sup> Zhejiang University <sup>2</sup> National University of Singapore

<sup>3</sup> State Street Technology (Zhejiang) Ltd. <sup>4</sup> Salesforce Research Asia

{lefeishen, chenmx, 11821003, xxren, sunjl, lizhuo}@zju.edu.cn  
 {liuxu726, twinsken}@gmail.com

## Abstract

Recent studies have revealed that vision models pre-trained on images can perform well in time series forecasting (TSF) by reformulating forecasting as an image reconstruction task, suggesting their potential as universal time series foundation models (TSFMs). However, effective cross-modal transfer from vision to time series remains challenging due to three key discrepancies: (1) the **data-modality gap** between structured, bounded image data and unbounded, heterogeneous time series; (2) the **multivariate-forecasting gap** between standard RGB three-channel-based vision models and the need to model time series with arbitrary numbers of variates; and (3) the **probabilistic-forecasting gap** between the deterministic output formats of most vision models and the requirement for uncertainty-aware probabilistic predictions. To bridge these gaps, we propose VISIONTS++, a vision-model-based TSFM that performs continual pre-training on large-scale time series datasets. Our approach introduces three core innovations: (1) a **vision-model-based filtering** mechanism to identify high-quality time series data, thereby mitigating modality gap and improving pre-training stability, (2) a **colorized multivariate conversion** method that transforms multivariate time series into multi-subfigure RGB images, capturing complex inter-variate dependencies; and (3) a **multi-quantile forecasting** approach using parallel reconstruction heads to generate forecasts of different quantile levels, thus more flexibly approximating arbitrary output distributions without restrictive prior distributional assumptions. Evaluated on both in-distribution and out-of-distribution TSF benchmarks, VISIONTS++ achieves state-of-the-art results, outperforming specialized TSFMs by 6%-44% in MSE reduction and ranking first in 9 out of 12 probabilistic forecasting settings. Our work establishes a new paradigm for cross-modal knowledge transfer, advancing the development of universal TSFMs. Code is available at <https://github.com/HALF111/VisionTSpp>.

## 1 Introduction

Foundation models have revolutionized natural language processing (NLP) [Devlin et al., 2019, Radford et al., 2019] and computer vision (CV) [Dosovitskiy et al., 2021, He et al., 2022, Liu et al., 2021], showcasing strong zero-shot capabilities. Inspired by this, time series forecasting (TSF) is shifting toward *universal forecasting* that can generalize across diverse forecasting scenarios without task-specific training, namely *time series foundation models* (TSFMs) [Woo et al., 2024, Ansari et al.,

\*Both authors contributed equally to this research. †Corresponding authors.

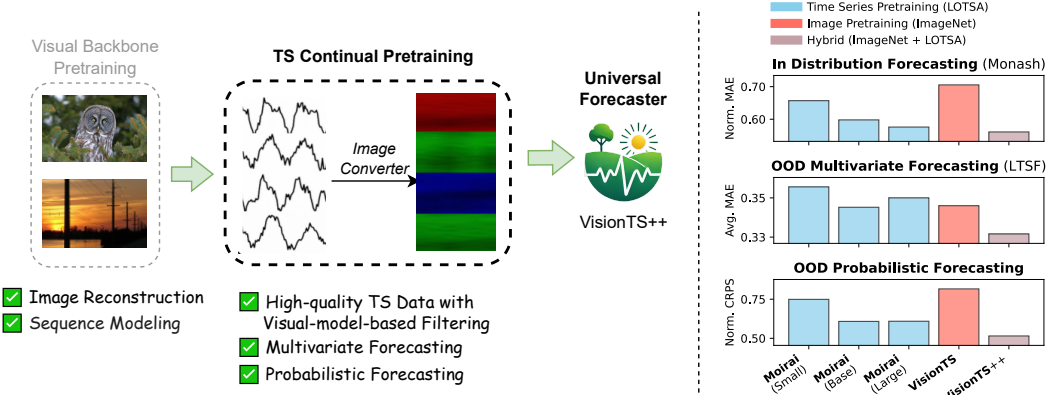


Figure 1: Left: Training process of VISIONTS++. We perform continual pre-training on a visual backbone (MAE) on high-quality large-scale time series datasets to make it a powerful TSFM, supporting diverse TSF capabilities including multivariate and probabilistic forecasting. Right: VISIONTS++ significantly outperforms MOIRAI and VISIONTS in both in-distribution and out-of-distribution multivariate probabilistic forecasting, demonstrating our model’s effectiveness.

2024, Das et al., 2024, Liu et al., 2024c, Goswami et al., 2024, Shi et al., 2024]. Unlike traditional methods that require separate models for each dataset, this emerging paradigm enables a one-fits-all solution by leveraging large-scale pre-training. However, unlike the standardized inputs/outputs in language and vision domains, the heterogeneity of time series data [Liu et al., 2024c, Ansari et al., 2024, Liu et al., 2024b] presents a major challenge for developing a unified foundation model.

Recent studies have discovered that image data can naturally serve as a valuable training source for TSFMs [Shen et al., 2025, Ni et al., 2025, Xu et al., 2025]. Notably, Chen et al. [2024a] demonstrates that by simply repurposing univariate TSF tasks as image reconstruction tasks, a visual MAE model that pre-trained totally on images exhibits powerful time series forecasting capabilities, sometimes even outperforming mainstream TSFMs. This transferability stems from the intrinsic similarities between images and time series: both originate from observations of real-world physical processes, and certain visual patterns (e.g., textures, structures) can conceptually map to temporal characteristics (e.g., trend, periodicity, stationarity).

However, despite this promise, some other key differences between images and time series limit further performance improvements. Specifically, we identify the following discrepancies: **Data-Modality Gap**: this gap arises from the mismatch between the structured, bounded nature of image data and the unbounded, heterogeneous characteristics of time series. Directly applying vision models to TSF without appropriate adaptation is therefore suboptimal. **Multivariate-Forecasting Gap**: vision models are typically designed for images with three color channels (R, G, B), which creates a mismatch with the arbitrary number of *variates* (also referred to as *channels* in this paper) in multivariate time series. This discrepancy hinders the effective modeling of inter-variate relationships; and **Probabilistic-Forecasting Gap**: most pre-trained vision models like MAE [He et al., 2022] primarily focus on deterministic point reconstruction or forecasting of image pixels, whereas practical TSFMs often require effective probabilistic forecasts that provide the measure of uncertainty [Woo et al., 2024, Ansari et al., 2024, Liu et al., 2024b].

A straightforward yet blunt approach to bridge these gaps involves invasive architectural modifications—such as replacing input/output layers with time series-specific encoders/decoders [Zhou et al., 2023, Jin et al., 2023, Ansari et al., 2024]—and subsequent continual pre-training on time series data. However, such methods can severely disrupt valuable pre-trained visual knowledge (leading to negative transfer [Chen et al., 2024a, Wang et al., 2019, Liu et al., 2024a]), and further degrade performance due to noisy or low-quality time series data [Liu et al., 2024c, Ansari et al., 2024]. For instance, Zhou et al. [2023] observed poor results from directly fine-tuning the vision model BeiT [Bao et al., 2021] for TSF. This raises a critical question: **How can we effectively adapt a pre-trained vision model for TSF tasks, maximizing transfer effectiveness while robustly preserving its original knowledge?**

Building upon the framework of VISIONTS, our model design philosophy is to minimally interfere with the MAE model structure, and to transform TSF tasks into image reconstruction tasks. Based

on this, we introduce VISIONTS++, a novel and strong vision-model based TSFM continual pre-trained on large-scale time series datasets, which supports flexible multivariate and probabilistic forecasting by efficiently transferring visual knowledge for TSF. Specifically, VISIONTS++ includes the following designs to bridge the gaps between images and time series.

- **Vision-Model-Based Filtering:** To bridge the *data-modality gap*, we introduce a filtering mechanism that leverages the vision model itself to select high-quality time series samples from large-scale pre-training datasets. Specifically, we discard samples that, when converted into images, are incompatible with the vision model’s input constraints—such as those exhibiting out-of-range values or abrupt, abnormal changes. This filtering process significantly reduces the risk of negative transfer and enables more stable continual pre-training.
- **Colorized Multivariate Conversion:** To address the *multivariate-forecasting gap*, we propose a method that reformulates multivariate time series forecasting as a multi-subfigure reconstruction task. Inspired by the structure of real-world images, often composed of multiple objects, we assign each variate to a distinct subfigure, analogous to an object within the image. This design enables inter-variante dependencies to be modeled as interactions between subfigures, aligning naturally with MAE’s native processing paradigm and its ability to analyze multi-object images.
- **Multi-Quantile Forecasting:** To address the *probabilistic forecasting gap*, we propose a multi-head forecasting strategy in which MAE generates multiple reconstructed images instead of one single image—each corresponding to a forecast of different quantile level—through parallel reconstruction heads. This effectively reformulates probabilistic forecasting as a set of point forecasts, better suited for vision models. Importantly, this approach makes full use of the pre-trained knowledge and offers flexible approximation of arbitrary output distributions, improving upon previous methods that rely on restrictive prior distributional assumptions [Woo et al., 2024].

After effective continual pre-training on large-scale time series datasets using the above approaches—which minimize critical gaps between images and time series while preserving useful visual knowledge—our VISIONTS++ achieves superior forecasting performance across both in-distribution and out-of-distribution scenarios. For in-distribution forecasting, VISIONTS++ surpasses all baseline methods, achieving the best normalized MAE on the Monash benchmark [Godahewa et al., 2021]. For out-of-distribution evaluations, VISIONTS++ significantly outperforms various time series foundation models by 6% - 44% in the reduction of MSE metric on the long-term TSF benchmark [Wu et al., 2021]. Moreover, it achieves top performance in 9 out of 12 evaluation settings on the Probabilistic Forecasting benchmark [Woo et al., 2024], demonstrating robust generalization across diverse forecasting tasks.

The training process and performance of VISIONTS++ are summarized in Figure 1. And our key contributions can be summarized as follows:

- We propose VISIONTS++, a novel TSFM that performs continual pre-training of vision models on large-scale time series datasets, effectively adapting the model to time series temporal patterns while preserving pre-trained visual knowledge.
- To better bridge critical gaps between images and time series, we introduce three core approaches for VISIONTS++: a vision-model-based filtering mechanism to address the data-modality gap, a colorized multivariate time series conversion method for the multivariate-forecasting gap, and a multi-quantile forecasting approach to tackle the probabilistic-forecasting gap.
- Extensive experiments demonstrate that VISIONTS++ achieves state-of-the-art performance across both in-distribution (e.g., Monash) and out-of-distribution (e.g., LTSF and PF) benchmarks, showcasing its superior forecasting accuracy and generalization ability.

## 2 Related Works

### 2.1 Time Series Foundation Models

Recent advances in time series forecasting have seen the emergence of time series foundation models (TSFMs) as powerful zero-shot forecasting tools. Unlike traditional dataset-specific models (e.g., PatchTST [Nie et al., 2022], TiDE [Das et al., 2023], FEDformer [Zhou et al., 2022]) that require training on target datasets, TSFMs leverage large-scale pre-training to achieve cross-domain

generalization. These models are typically pre-trained on diverse real-world time series datasets across diverse domains [Goswami et al., 2024, Liu et al., 2024c, Das et al., 2024, Dong et al., 2024, Feng et al., 2024] or pre-trained on synthetic time series data [Liu et al., 2025b, Fu et al., 2024, Yang et al., 2024a]. Notable examples include Moirai [Woo et al., 2024], which assembles a data archive of 231 billion observations across nine domains to train encoder-based models of varying scales, demonstrating strong zero-shot capabilities. Other foundation models with mostly encoder-based or decoder-based architectures have shown similar success, including Chronos [Ansari et al., 2024], TimesFM [Das et al., 2024], Timer [Liu et al., 2024c], Moment [Goswami et al., 2024], and TimeMoE [Shi et al., 2024]. However, developing an effective TSFM faces significant challenges due to the inherent heterogeneity and high noise in time series data, thus demanding the construction of high-quality training datasets.

## 2.2 Vision Models for Time Series Analysis

The exploration of vision-model-based approaches for time series analysis has significantly progressed in recent years. Early works demonstrate that encoding time series as images enables effective application of convolutional neural networks (CNNs) for both classification [Wang and Oates, 2015a,b, Hatami et al., 2018] and forecasting tasks [Li et al., 2020, Sood et al., 2021, Semenoglou et al., 2023]. More recent advances have started to leverage pre-trained visual foundation models or vision-language models for time series analysis. For instance, AST [Gong et al., 2021] adopts DeiT [Touvron et al., 2021] for time series classification, and ViTST [Li et al., 2023] utilizes pre-trained vision transformers (ViTs) [Dosovitskiy et al., 2021] and swin transformers [Liu et al., 2021] to further explore this direction. Other works, such as Wimmer and Rekabsaz [2023] and Zhang et al. [2023], explore the use of vision-language models for feature extraction and textual description generation. Moreover, ViTime [Yang et al., 2024a] generates synthetic time series data and converts them into line plots for pre-training vision models such as ViT. ImagenTime [Naiman et al., 2024] introduces a unified generative framework by transforming time series into images via invertible methods like delay embedding and STFT, enabling them to leverage advanced vision diffusion models for generation, interpolation, and extrapolation tasks. Several recent surveys [Ni et al., 2025, Jiang et al., 2025, Liu et al., 2025a, Xu et al., 2025] have also discussed the application of vision models or multi-modal approaches in time series analysis. For example, Vision4TS [Ni et al., 2025] summarizes crucial techniques including time-series-to-image transformation, image pre-processing, and modeling strategies for imaged time series. The most relevant approach is VISIONTS [Chen et al., 2024a], which reformulates time series forecasting as a patch-level image reconstruction task and leverages the visual MAE model as the backbone.

However, although these methods establish preliminary connections between visual and time series domains, they fail to sufficiently address some critical modality gaps. To the best of our knowledge, we are the first to propose a competitive TSFM through continual pretraining on vision backbones, thus better enhancing the transferability between two modalities.

## 3 Preliminaries

**Time Series Forecasting (TSF)** We begin by defining time series forecasting. For a multivariate time series with  $M$  variates (also referred to as *channels* in this paper), let  $\mathbf{x}_t \in \mathbb{R}^M$  represent the value at  $t$ -th time step. Then given a historical sequence (*i.e.*, look-back window)  $\mathbf{X}_{t-L:t} = [\mathbf{x}_{t-L}, \dots, \mathbf{x}_{t-1}] \in \mathbb{R}^{L \times M}$  with a context length of  $L$ , the TSF task is to use  $\mathbf{X}_{t-L:t}$  to predict future values (*i.e.*, forecasting window):  $\hat{\mathbf{X}}_{t:t+T} = [\hat{\mathbf{x}}_t, \dots, \hat{\mathbf{x}}_{t+T-1}] \in \mathbb{R}^{T \times M}$ , where  $T$  is the prediction length.

**Image Reconstruction Task** To effectively obtain visual representation for downstream CV tasks, the masked autoencoder model (MAE) [He et al., 2022] is proposed to pre-train a Vision Transformer (ViT) [Dosovitskiy et al., 2021] with an image reconstruction task on the ImageNet dataset. Specifically, for an image of size  $W \times W$  (where  $W$  represents both the width and height, since images in ImageNet are square), the image is evenly divided into  $N \times N$  patches, each with a width and height of  $S = W/N$ . During pre-training, some random patches are masked, while the remaining *visible patches* are fed into the ViT model. MAE models are trained to reconstruct the masked pixel values based on these visible patches.

**Quick Review of VISIONTS** Before introducing VISIONTS++, we briefly revisit the key methodology of VISIONTS [Chen et al., 2024a]. Its core idea is to reformulate the TSF task as a patch-level image reconstruction task by transforming a 1D time series into a 2D image, thereby enabling the use of visual foundation models like MAE as the backbone. This reformulation involves five key steps: (1) Segmentation and Image Conversion: given a 1D univariate time series data  $X \in \mathbb{R}^L$ , it is firstly segmented into  $\lfloor L/P \rfloor$  subsequences of periodicity length  $P$  considering the cyclical patterns. The 1D time series is then converted into a 2D image by stacking these subsequences into a 2D matrix, *i.e.*,  $I_{\text{raw}} \in \mathbb{R}^{P \times \lfloor L/P \rfloor}$ . (2) Normalization:  $I_{\text{raw}}$  is applied with instance normalization, yielding  $I_{\text{norm}}$  with the same shape. (3) Rendering:  $I_{\text{norm}}$  is then rendered into a grayscale image  $I_{\text{grey}} \in \mathbb{R}^{P \times \lfloor L/P \rfloor \times 3}$  by repeating values across all three RGB channels. (4) Alignment: to match the standard image size,  $I_{\text{grey}}$  is resampled via bilinear interpolation from original dimensions  $(P, \lfloor L/P \rfloor)$  to  $(N \cdot S, n \cdot S)$  by bilinear interpolation, where  $S$  is patch size,  $N$  is number of patches, and  $n = \lfloor N \cdot L/(L+T) \rfloor$  is determined by the ratio of context length  $L$  to prediction length  $T$ . The resized image is treated as the “visible” left portion, with the right portion masked for prediction. (5) Reconstruction and Time-series Conversion: the MAE-reconstructed image is converted to a 1D time series by reversing the previous steps, including resizing, channel averaging, de-normalizing, and flattening by periodicity.

## 4 Methodology

In this section, we present the main framework of VISIONTS++. Building upon VISIONTS, we reformulate the TSF task as an image reconstruction problem and further enhance it by continually pre-training the vision model on large-scale time series datasets. Such pre-training enables the vision model to better conform to the distribution of various time series data, improving its application across diverse downstream TSF domains. Nevertheless, straightforward continual pre-training alone remains insufficient to bridge several critical gaps between images and time series, including the *data-modality gap*, *multivariate-forecasting gap*, and *probabilistic-forecasting gap*, which can severely hinder cross-modal transferability. To effectively address these challenges, we propose targeted modifications and novel designs to facilitate the continual pre-training process as well as the transferability between two modalities. We elaborate on these designs in the following sections. The overall framework of VISIONTS++ is illustrated in Figure 2.

### 4.1 Vision-model-based Filtering for Time Series Pre-training Data

Firstly, to address the **data-modality gap**—the fact that many real-world images lack time series characteristics and therefore provide limited value for TSF tasks—the core idea of our VISIONTS++ is to enhance the visual foundation model by continual pre-training on large-scale time series data. This enables the vision model to better adapt to the distribution of time series data.

However, directly leveraging these large-scale time series datasets is suboptimal, since the inherent heterogeneity and high noise in the data raise concerns about data quality [Liu et al., 2024c, Ansari et al., 2024, Shi et al., 2024], thus demanding effective data curation approaches. To obtain high-quality datasets, prior work in language models [Albalak et al., 2024, Goyal et al., 2024, Marion et al., 2023] and vision-language models [Chen et al., 2024b, Fang et al., 2023, Radenovic et al., 2023] has demonstrated that data filtering strategies can significantly improve dataset quality. Inspired by these successes, we explore the feasibility of applying similar techniques to time series data—but a key question arises: **“How can we effectively filter low-quality time series to better bridge the data-modality gap for vision models?”**

Our core idea is to leverage the vision model itself to identify and filter out those low-quality time series. Notably, we observe that vision models expect inputs within a bounded range (*e.g.*, image raw pixels in  $[0, 255]$ ), whereas time series values are often unbounded. Time series containing out-of-range values may interfere with the model’s pre-trained visual knowledge, reducing its transfer effectiveness. To address this, we propose a **“vision-model-based filtering”** approach for the time series pre-training data (see bottom left part of Figure 2), which retains only samples compatible with the vision model’s input constraints.

Specifically, since image pixel values are bounded between 0 and 255, assuming the mean and standard deviation of the pre-trained image dataset (*e.g.*, ImageNet) used by the vision model are  $I_{\text{mean}}$  and  $I_{\text{std}}$  respectively, all valid image data fall within the range  $[(0 - I_{\text{mean}})/I_{\text{std}}, (255 - I_{\text{mean}})/I_{\text{std}}]$  after normalization. Then for a given time series input  $X_{t-L:t} \in \mathbb{R}^{L \times M}$  and target  $\hat{X}_{t:t+T} \in \mathbb{R}^{T \times M}$ , we

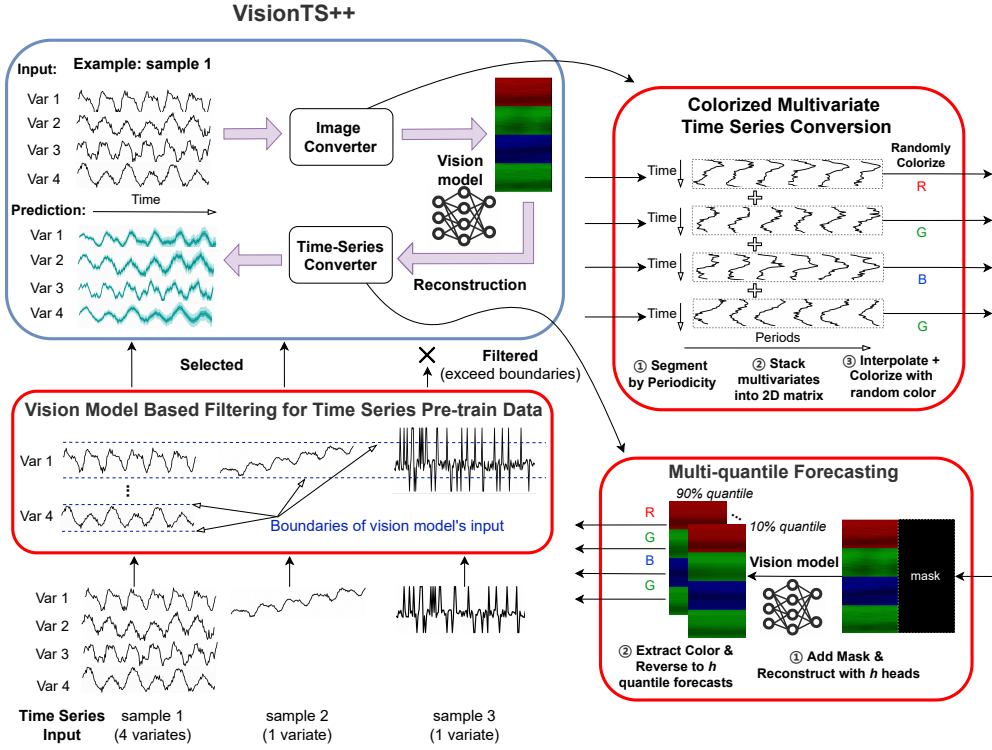


Figure 2: Main Framework of VISIONTS++. For each input time series sample, the following pipeline is applied: (1) **Vision-Model-Based Filtering**: Time series sample containing abnormal mutations that exceed the vision model’s input range constraints are filtered out. (2) **Colorized Multivariate Time Series Conversion**: The multivariate time series is segmented by its periodicity and reshaped into a 2D format, where each variate is randomly assigned a distinct color to enhance inter-variate separation. (3) **Multi-Quantile Forecasting**: After reconstruction by the vision model, multiple parallel projection heads map the reconstructed image into forecasts at different quantiles levels to support probabilistic forecasting.

calculate the mean  $\mathbf{X}_{mean}$  and standard deviation  $\mathbf{X}_{std}$  of  $\mathbf{X}_{t-L:t}$ , and use them to normalize both the input and target.

Notably, similar to VISIONTS, when preparing the normalized time series for conversion into images, we further scale it by a factor  $r < 1$ . This scaling aligns two modalities by accounting for their statistical differences. VISIONTS found that  $r = 0.4$  yields the best performance, which can be interpreted as the ratio of standard deviations between two modalities, and we adopt this value accordingly. As a result, the final normalized time series data becomes:  $\mathbf{X}_{t-L:t}^{norm} = r \cdot \frac{\mathbf{X}_{t-L:t} - \mathbf{X}_{mean}}{\mathbf{X}_{std}}$  and  $\mathbf{X}_{t:t+T}^{norm} = r \cdot \frac{\mathbf{X}_{t:t+T} - \mathbf{X}_{mean}}{\mathbf{X}_{std}}$ . However, even after such scaling for aligning two modalities, the resulting images may still exceed the valid pixel boundaries expected by the vision model. To address this issue, we discard any samples whose normalized values fall outside the previously defined visual data range. Therefore, we use the visual data range as a filtering criterion: if all values in the normalized input  $\mathbf{X}_{t-L:t}^{norm}$  and target  $\mathbf{X}_{t:t+L}^{norm}$  lie within the above range  $[(0 - I_{mean})/I_{std}, (255 - I_{mean})/I_{std}]$ , the sample is accepted for pre-training; otherwise, it is filtered out to ensure compatibility with the vision model’s input constraints.

## 4.2 Colorized Multivariate Time Series Conversion for Image Converter

After selecting high-quality time series samples for the continual pre-training, we first need an image converter to transform 1D time series sequences into 2D images before feeding them into the visual backbone model. However, one limitation of VISIONTS is that it converts each variate of multivariate time series into separate images and processes them independently. While such channel independence strategy [Nie et al., 2022] is effective in certain scenarios, it incurs higher computational cost and

fails to capture the potential relationships between variates. In contrast, a universal foundation model should be capable of efficiently and effectively handling arbitrary multivariate time series [Woo et al., 2024, Shi et al., 2024]. This leads to a critical question: **“How can we extend the image-based approach to better support efficient and effective multivariate time series forecasting?”**

A straightforward solution is to utilize the vision model’s RGB channels as carriers for the multiple variates. However, there exists a significant “**Multivariate-Forecasting Gap**” between them: standard vision models are designed with three channels to match the RGB structure of images, which cannot naturally accommodate the high dimension of time series with arbitrary numbers of variates.

To address this issue, we draw inspiration from vision models’ inherent ability to process multiple objects with clear boundaries within a single image. Although colors (*i.e.*, RGB channels) cannot serve as carriers for multiple variates, **subfigures can**. We can map each variate of a time series into a fraction of an image to tackle the problem. Instead, RGB color channels do not carry the multiple variates themselves but function as providing clear boundaries between variates. These insights lead us to develop our “Colorized Multivariate Time Series Conversion” method, illustrated in the top right portion of Figure 2.

Specifically, for a multivariate input  $\mathbf{X}_{t-L:t} \in \mathbb{R}^{L \times M}$ , we follow VISIONTS and first segment it into  $\lfloor \frac{L}{P} \rfloor$  subsequences using length  $P$  for each of  $M$  variates, where  $P$  is the periodicity length. After that, we stack these subsequences into a 2D matrix in the shape of  $P \times \lfloor \frac{L}{P} \rfloor$  for each of  $M$  variates, obtaining  $\mathbf{I}_{\text{raw}} \in \mathbb{R}^{M \times P \times \lfloor \frac{L}{P} \rfloor}$ .

The conversion process continues by resampling each variate’s 2D matrix from  $(P, \lfloor \frac{L}{P} \rfloor)$  to  $(\lfloor \frac{W}{M} \rfloor, W/2)$ . It is worth noting that we fix the width of both left visible part and right masked part as 50% of the image width (*i.e.*,  $W/2$ ), which is different from VISIONTS. This setting facilitates efficient batch training on heterogeneous time-series samples with varying look-back and prediction window lengths. Afterwards, we vertically concatenate all  $M$  variates into  $(\lfloor \frac{W}{M} \rfloor \times M, W/2)$ , aligning with the left visible portion of the image. In case  $M$  is not evenly divided by  $W$ , zero-padding will be made at the bottom of the images. By representing each variate as a distinct subfigure within a complete image, we transform the modeling of variate interactions into a task of multi-object analysis and patch-level attention, which are more familiar and amenable to vision models. This enables VISIONTS++ to better capture the inter-variante dependencies in the multivariate time series.

Furthermore, to ensure clear boundaries between variates, we implement an innovative colorized channel strategy. For each variate (subfigure), it is randomly assigned to one of the three RGB channels, with the other two channels set to zero values. Crucially, we enforce that adjacent subfigures use different color channels to prevent confusion. This colorization scheme serves two important purposes: first, it creates explicit boundaries that activate the vision model’s native multi-object analysis capabilities; second, the randomized color assignment trains the model to recognize color as a boundary indicator rather than focusing on specific color values.

### 4.3 Multi-quantile Forecasting for Time Series Converter

After obtaining the converted image, we apply a mask matrix on the right portion and feed it into the visual backbone model for image reconstruction. Although this deterministic reconstruction provides a point estimate of future values, it fails to capture forecast uncertainty and complete probabilistic forecasting, which is a key requirement in most TSFMs [Woo et al., 2024, Ansari et al., 2024]. This limitation arises from a fundamental mismatch: most vision models are primarily designed for deterministic tasks like classification or pixel-level reconstruction, and thus do not inherently support probabilistic outputs. Although some vision models support probabilistic outputs (*e.g.*, through Bayesian formulations or ensemble methods), these methods are not specifically aligned with the temporal and stochastic nature of time series forecasting. Even when prior works like VISIONTS invert the reconstructed image back into time series, they produce single-point forecasts, falling short in addressing the **Probabilistic-Forecasting Gap**. To enable robust uncertainty quantification in our vision-based TSFM, we are led to a critical question: **“How can we transform the deterministically reconstructed image into meaningful probabilistic forecasts that accurately reflect the uncertainty in future time series?”**

To bridge this gap, we propose a novel “**Multi-quantile Forecasting**” approach for the time series converter that extends the capabilities of the vision model, presented in the bottom right part of Figure 2. Drawing inspiration from statistical strategies, we leverage multi-quantile estimation to

approximately characterize the full forecast distribution [Wen et al., 2017, Gasthaus et al., 2019, Park et al., 2022, Lim et al., 2021]. Specifically, we modify the standard framework by introducing parallel forecasting heads, each trained to generate image reconstructions corresponding to specific quantile levels of the forecast distribution. For the model with  $h$  forecasting heads, we assign them to evenly spaced quantile levels  $[1/(h+1), 2/(h+1), \dots, h/(h+1)]$ . Each head is supervised using the corresponding quantile loss (see Section 4.4), enabling it to learn distinct aspects of the predictive uncertainty at its assigned level. This design ensures broad coverage across both tails and central regions of the predicted distribution.

Specifically, the image-to-time-series conversion process starts by vertically separating the reconstructed image by  $\lfloor W/M \rfloor$  into  $M$  variates for each of  $h$  outputs. Each variate’s values are extracted from its designated RGB channel according to the above colorization scheme, and then resampled from  $(\lfloor W/M \rfloor, W/2)$  to  $(P, \lfloor T/P \rfloor)$  to restore the original periodic structure. Finally, we recompose these  $M$  variates into the time series of shape  $(T, M)$  for each of  $h$ -heads’ outputs, thus generating complete probabilistic forecasts spanning the desired prediction horizon.

Unlike methods that necessitate explicit probabilistic modeling—whether through parametric distributions (e.g., Gaussian, Student’s t) [Flunkert et al., 2017, Woo et al., 2024] or complex generative processes (e.g., diffusion models that implicitly learn distributions) [Meijer and Chen, 2024, Li et al., 2022, Yang et al., 2024b]—our approach ingeniously leverages the vision model’s native pixel reconstruction capability. This design circumvents the need for forcibly incorporating distribution knowledge, offering several compelling advantages: (1) Seamless Transfer Learning: It directly leverages the powerful representations from visual pre-trained models for probabilistic forecasting, with minimal domain-specific architectural alterations. (2) Distribution-Free Quantile Estimation: By relying on pixel-level reconstruction, our approach inherently avoids restrictive assumptions about the underlying data distribution, a common bottleneck in traditional methods. (3) Flexible Uncertainty Quantification: It provides highly adjustable uncertainty quantification through a varied number of forecasting heads, precisely capturing diverse uncertainty levels crucial for decision-making. The resulting framework naturally supports both comprehensive probabilistic forecasting via quantile estimations and robust point forecasting through median predictions, demonstrating remarkable versatility across different forecasting requirements.

#### 4.4 Training Objective

Finally, we employ a quantile loss function as our training objective, which simultaneously evaluates all  $h$  forecasting outputs. This approach provides comprehensive supervision by assessing model performance across different quantile levels of the predicted distribution.

Specifically, given  $h$  quantile levels of  $[1/(h+1), 2/(h+1), \dots, h/(h+1)]$  and  $h$  forecasting results represented as  $\left[ \mathbf{X}_{t:t+T}^{(1)}, \mathbf{X}_{t:t+T}^{(2)}, \dots, \mathbf{X}_{t:t+T}^{(h)} \right]$ , along with the ground truth  $\hat{\mathbf{X}}_{t:t+T}$ , we first compute the error term  $\mathbf{E}_i$  between ground truth and  $i$ -th prediction and then the pinball loss  $l_i$  for corresponding  $i$ -th quantile level. The final training objective  $\mathcal{L}_q$  combines all quantile-specific losses through averaging, represented as follows:

$$q_i = i/(h+1), \quad \mathbf{E}_i = \hat{\mathbf{X}}_{t:t+T} - \mathbf{X}_{t:t+T}^{(i)}, \quad l_i = \max(q_i \cdot \mathbf{E}_i, (q_i - 1) \cdot \mathbf{E}_i), \quad i \in \{1, 2, \dots, h\},$$

$$\mathcal{L}_q = \sum_{i=1}^h 1/h \cdot l_i$$

This quantile loss is well-suited for VISIONTS++ as it aligns with the probabilistic nature of our forecasting approach. It offers several benefits, such as ensuring balanced training across the entire predicted distribution rather than focusing on a single point estimation, as well as enabling joint optimization of all forecasting heads while preserving their distinct quantile-specific characteristics.

### 5 Experiments

#### 5.1 Experimental Setup

**Training Dataset.** Firstly, we employ the Large-scale Open Time Series Archive (LOTSA) dataset to continually pre-train our VISIONTS++, which is commonly used by many time series foundation

models [Woo et al., 2024, Liu et al., 2024b]. The LOTSA dataset comprehensively covers time series from various domains and contains over 231 billion observations. Such a large-scale dataset provides the breadth and depth necessary to develop robust time series forecasting capabilities.

**Model Architecture.** Our VISIONTS++ model builds upon the MAE (base) architecture [He et al., 2022] with 112 million parameters as our backbone, initialized with pre-trained weights on the ImageNet. For comprehensive analysis, we also evaluate larger variants (MAE (large) with 330M and MAE (huge) with 657M parameters) in Section 5.4.

Beyond the MAE backbone,  $h$  for the “multi-quantile forecasting” component is set to 9, targeting decile quantile levels of  $[10\%, 20\%, \dots, 90\%]$  to achieve approximate distribution estimation without excessive complexity.

**Training Process and Optimization Strategy.** The continual pre-training process runs for 100,000 steps with a batch size of 512, ensuring sufficient exposure to diverse temporal patterns. Meanwhile, we employ the AdamW optimizer [Loshchilov and Hutter, 2017] with following parameters: learning rate of 1e-4, weight decay of 1e-2, and momentum terms  $\beta_1 = 0.9$ ,  $\beta_2 = 0.98$ . The learning rate follows a schedule combining linear warm-up for the first 10,000 steps with subsequent cosine annealing, promoting stable training and effective convergence. Notably, we update all model parameters during continual pre-training to better adapt the visual representations to TSF tasks.

**Evaluation Protocol.** Our experiments follow established protocols from recent foundation model research [Woo et al., 2024, Chen et al., 2024a, Liu et al., 2024b], evaluating on three key benchmarks: (1) Monash [Godahewa et al., 2021], (2) Long-term Time Series Forecasting (LTSF) [Wu et al., 2021], and (3) Probabilistic Forecasting (PF) [Woo et al., 2024]. These benchmarks are compatible with the pre-trained LOTSA dataset, which avoids the potential data leakage and provides comprehensive assessments across multiple forecasting scenarios. Additionally, our experiments comprehensively compare VISIONTS++ against state-of-the-art foundation models, various deep learning, and traditional baselines (see Appendix A for details). Specifically, among these baselines, we mainly focus on two representative models, VISIONTS (ImageNet pre-trained) and MOIRAI (LOTSA time series pre-trained), to highlight key aspects of our approach. Different from them, VISIONTS++ first uses an MAE model pre-trained on ImageNet, then undergoes continual pre-training on LOTSA. This unique design enables us to validate the critical role of continual pre-training for adapting vision models to temporal data. (vs. VISIONTS) and demonstrate the significant benefits of visual pre-training for time series forecasting (vs. MOIRAI).

## 5.2 In-distribution Forecasting

**Monash Time Series Forecasting.** Firstly, we conduct experiments on a total of 29 datasets from the Monash Benchmark [Godahewa et al., 2021] for an in-distribution evaluation, which we describe in detail in Appendix A.1. This evaluation follows rigorous protocols where the pre-training dataset LOTSA contains only the training portions of Monash datasets, while the held-out test sets are reserved exclusively for evaluation.

Figure 3 summarizes the normalized mean absolute error (normalized MAE) for all models and baselines. This metric first scales each model’s MAE relative to a naive forecasting baseline for individual datasets, then computes the geometric mean across all datasets. The experimental results demonstrate VISIONTS++’s superior forecasting capability on the Monash benchmark. First, our model consistently outperforms both dataset-specific models and the original VISIONTS with performance improvements over 23.2%, validating the effectiveness of our proposed pre-training paradigm. More significantly, VISIONTS++ achieves better performance than the foundation model MOIRAI across all three model sizes, even though both models are trained on the same Monash training set. Since in-distribution evaluations primarily assess the model’s ability to memorize the training distribution, these superior results suggest that: pre-trained vision model weights and visual knowledge provide a strong initialization for TSFMs. Compared to MOIRAI models trained from scratch, VISIONTS++ can converge faster and thus learn patterns in the training data more efficiently.

## 5.3 Out-of-distribution Forecasting

To further evaluate the generalization capability of VISIONTS++, we conduct comprehensive out-of-distribution forecasting (*i.e.*, zero-shot forecasting) experiments on two widely-used benchmarks

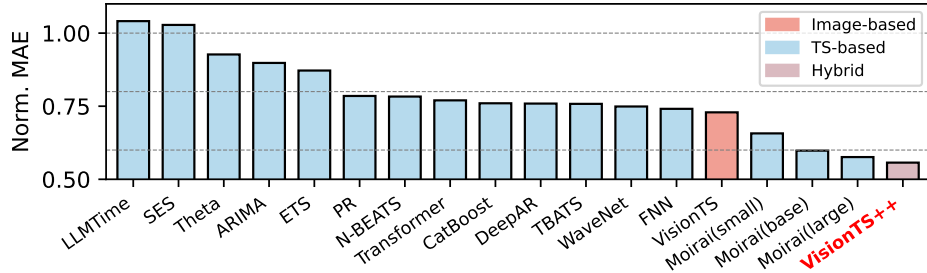


Figure 3: Comparative performance on Monash Benchmark showing normalized MAE, with complete results for individual datasets reported in Table 6 in Appendix B.1.

(LTSF and PF) where neither train nor test data overlaps with our pre-training dataset LOTSA. This evaluation framework tests the model’s ability to transfer learned patterns to unseen domains and novel forecasting scenarios.

**Long-term Time Series Forecasting (LTSF).** We first evaluate on the standard LTSF benchmark introduced by Wu et al. [2021], comparing against state-of-the-art time series foundation models including VisionTS [Chen et al., 2024a], Time-MoE [Shi et al., 2024], Chronos [Ansari et al., 2024], Moirai [Woo et al., 2024], Moment [Goswami et al., 2024], Timer [Liu et al., 2024c], and TimesFM [Das et al., 2024]. Table 1 presents aggregated results (averaged across four prediction lengths {96, 192, 336, 720}) using both Mean Squared Error (MSE) and Mean Absolute Error (MAE) metrics, with complete results available in Table 7 in Appendix B.2.

The experimental results reveal several key insights. First, VISIONTS++ achieves superior performance in 12 out of 14 evaluation scenarios, demonstrating consistent advantages across diverse datasets. Notably, it shows a 6% average MSE improvement over VISIONTS, validating that our framework modifications and the continual pre-training process successfully preserve valuable visual knowledge while enhancing time series forecasting capabilities. More remarkably, VISIONTS++ outperforms specialized time series foundation models by 6%-44% in MSE, suggesting that through our dedicated designs, the continually pre-trained vision model addresses multiple gaps between images and time series, demonstrating superior time series forecasting capability, and further validating the cross-modal transferability.

Table 1: Zero-shot results on the long-term TSF benchmark. Results are averaged across four prediction lengths {96, 192, 336, 720}, with full results in Table 7 (Appendix B.2). The subscripts after the model name refers to the model size, (*i.e.*, **s**: small, **b**: base, **l**: large). Best results are highlighted in **bold**. Since either Electricity or Weather are included in the pre-trained datasets for Time-MoE, Timer, and TimesFM, we are not able to report their zero-shot results.

Dataset	Method	Pre-train				Time-Series								
		VisionTS++	VisionTS	Time-MoE <sub>s</sub>	Time-MoE <sub>b</sub>	Chronos <sub>s</sub>	Chronos <sub>b</sub>	Chronos <sub>l</sub>	Moirai <sub>s</sub>	Moirai <sub>b</sub>	Moirai <sub>l</sub>	Moment	Timer <sub>2SB</sub>	TimesFM
ETTm1	MSE	<b>0.360</b>	0.374	0.394	0.376	0.640	0.646	0.556	0.448	0.382	0.390	0.670	0.487	0.433
	MAE	<b>0.372</b>	0.372	0.416	0.406	0.500	0.500	0.465	0.410	0.388	0.389	0.537	0.457	0.419
ETTm2	MSE	<b>0.244</b>	0.282	0.318	0.316	0.349	0.310	0.295	0.300	0.272	0.276	0.317	0.316	0.328
	MAE	<b>0.298</b>	0.321	0.366	0.361	0.380	0.350	0.338	0.341	0.321	0.320	0.366	0.371	0.347
ETTh1	MSE	0.402	<b>0.390</b>	0.400	0.394	0.545	0.591	0.589	0.400	0.434	0.510	0.684	0.444	0.473
	MAE	0.416	<b>0.414</b>	0.424	0.420	0.472	0.468	0.466	0.424	0.439	0.469	0.566	0.457	0.444
ETTh2	MSE	<b>0.333</b>	<b>0.333</b>	0.367	0.405	0.424	0.406	0.455	0.341	0.346	0.354	0.362	0.358	0.392
	MAE	<b>0.370</b>	0.375	0.404	0.415	0.430	0.411	0.427	0.379	0.382	0.377	0.410	0.407	0.406
Electricity	MSE	<b>0.184</b>	0.207	-	-	0.220	0.215	0.204	0.233	0.188	0.188	0.765	-	-
	MAE	<b>0.265</b>	0.294	-	-	0.284	0.279	0.274	0.320	0.274	0.273	0.687	-	-
Weather	MSE	<b>0.222</b>	0.269	0.266	0.270	0.300	0.293	0.279	0.242	0.238	0.260	0.294	0.304	-
	MAE	<b>0.241</b>	0.292	0.297	0.300	0.318	0.315	0.306	0.267	0.261	0.275	0.326	0.331	-
Average	MSE	<b>0.291</b>	0.309	-	-	0.413	0.410	0.396	0.327	0.310	0.329	0.515	-	-
	MAE	<b>0.327</b>	0.345	-	-	0.397	0.387	0.379	0.357	0.344	0.350	0.482	-	-
1 <sup>st</sup> count		12	4	0	0	0	0	0	0	0	0	0	0	0

**Probabilistic Forecasting (PF).** We further assess probabilistic forecasting capabilities using the PF benchmark [Woo et al., 2024], which includes six real-world datasets across energy, transport, climate, and sales domains. We report the Continuous Ranked Probability Score (CRPS) as the probabilistic forecasting metric, and the Mean Absolute Scaled Error (MASE) as the point forecasting metric of VISIONTS++ against various zero-shot, full-shot, and simple baselines in Table 2.

Table 2: Zero-shot results on the probabilistic forecasting benchmark. Best results are highlighted in **bold** texts.

Dataset	Method	Zero-shot				Full-shot			Baseline	
		VisionTS++	VisionTS	Moirai <sub>a</sub>	Moirai <sub>b</sub>	PatchTST	TIDE	TFT	DeepAR	AutoARIMA
Electricity	CRPS	<b>0.042</b>	0.068	0.072	0.055	0.050	0.052±0.00	0.048±0.00	0.050±0.00	0.065±0.01
	MASE	<b>0.631</b>	0.755	0.981	0.792	0.751	0.753±0.01	0.706±0.02	0.747±0.03	0.844±0.16
Solar	CRPS	<b>0.353</b>	0.502	0.471	0.419	0.406	0.518±0.09	0.420±0.00	0.446±0.03	0.431±0.01
	MASE	1.155	<b>1.141</b>	1.465	1.292	1.237	1.607±0.25	1.265±0.02	1.399±0.11	1.222±0.01
Walmart	CRPS	<b>0.064</b>	0.121	0.103	0.093	0.098	0.082±0.01	0.077±0.00	0.087±0.00	0.121±0.00
	MASE	<b>0.689</b>	0.949	1.048	0.964	1.007	0.867±0.09	0.814±0.01	0.948±0.02	1.193±0.02
Weather	CRPS	<b>0.038</b>	0.056	0.049	0.041	0.051	0.059±0.01	0.054±0.00	0.043±0.00	0.132±0.11
	MASE	<b>0.447</b>	0.737	0.521	0.487	0.515	0.844±0.19	0.832±0.13	0.692±0.02	3.170±3.47
Istanbul Traffic	CRPS	0.115	0.198	0.173	0.116	0.112	0.112±0.00	0.110±0.01	0.110±0.01	<b>0.108±0.00</b>
	MASE	0.616	0.706	0.990	0.644	0.631	0.653±0.02	0.618±0.03	0.620±0.03	<b>0.613±0.03</b>
Turkey Power	CRPS	<b>0.036</b>	0.052	0.048	0.040	<b>0.036</b>	0.054±0.01	0.046±0.01	0.039±0.00	0.066±0.02
	MASE	<b>0.737</b>	0.856	0.948	0.888	0.870	1.234±0.12	0.904±0.02	0.890±0.05	1.395±0.30
<b>1<sup>st</sup> count</b>		9	1	0	0	1	0	0	0	2
									0	0

Table 3: Random initialization (right) vs. Loading MAE pre-trained weights (left) before CPT.

		VisionTS++ rand_init	
Monash	MAE	<b>0.561</b>	0.733
PF	MASE	<b>0.677</b>	0.814
	CRPS	<b>0.515</b>	0.627
ETTm1	MSE	<b>0.360</b>	0.387
	MAE	<b>0.372</b>	0.396
ETTm2	MSE	<b>0.244</b>	0.29
	MAE	<b>0.298</b>	0.337
ETTh1	MSE	<b>0.402</b>	0.447
	MAE	<b>0.416</b>	0.45
ETTh2	MSE	<b>0.333</b>	0.47
	MAE	<b>0.370</b>	0.439
Electricity	MSE	<b>0.184</b>	0.225
	MAE	<b>0.265</b>	0.298
Weather	MSE	<b>0.222</b>	0.233
	MAE	<b>0.241</b>	0.257

Table 4: Ablation studies on each component in the VISIONTS++.

		VisionTS++	w/o filter	w/o color	w/o quantile
Monash	MAE	<b>0.561</b>	0.593	0.578	0.634
PF	MASE	<b>0.677</b>	0.714	0.690	0.725
	CRPS	<b>0.515</b>	0.551	0.531	0.565
ETTm1	MSE	<b>0.360</b>	0.392	0.388	0.408
	MAE	<b>0.372</b>	0.401	0.397	0.419
ETTm2	MSE	<b>0.244</b>	0.278	0.270	0.302
	MAE	<b>0.298</b>	0.328	0.324	0.356
ETTh1	MSE	<b>0.402</b>	0.421	0.416	0.453
	MAE	<b>0.416</b>	0.438	0.425	0.464
ETTh2	MSE	<b>0.333</b>	0.355	0.336	0.376
	MAE	<b>0.370</b>	0.387	0.372	0.402
Electricity	MSE	<b>0.184</b>	0.208	0.189	0.215
	MAE	<b>0.265</b>	0.288	0.272	0.299
Weather	MSE	<b>0.222</b>	0.234	0.228	0.245
	MAE	<b>0.241</b>	0.259	0.249	0.271

Based on the results, VISIONTS++ achieves top performance in 9 out of 12 evaluation scenarios according to both CRPS and MASE metrics. The results highlight three important findings: Firstly, VISIONTS++ significantly improves upon VISIONTS in probabilistic forecasting, demonstrating the effectiveness of our multi-quantile forecasting approach. Secondly, VISIONTS++ outperforms both zero-shot and full-shot baselines, showing robust generalization without dataset-specific tuning. Lastly, even in the single case (Istanbul Traffic) where a full-shot baseline performs slightly better, VISIONTS++’s zero-shot performance remains highly competitive.

The results indicate that our approach successfully narrows the probabilistic forecasting gap between vision and time series modalities. Moreover, it achieves state-of-the-art performance in out-of-distribution settings. This demonstrates that, with appropriate continual pre-training through our method, visual foundation models can surpass specialized TSF models in terms of probabilistic forecasting ability and generalization ability.

#### 5.4 Further Analysis on VISIONTS++

**Random Initialization.** Firstly, to validate the contribution of visual knowledge in MAE’s original pre-trained weights to downstream TSF tasks, we compare the performance between VISIONTS++ and the model with a randomly initialized MAE backbone in Table 3. Specifically, the former model loads the original weights (pre-trained on ImageNet) before continual pre-training on time series, while the latter one randomly initializes MAE’s parameters.

The results reveal significant performance degradation (about 30% aggregated on each metric) when using random initialization, conclusively demonstrating that the original visual knowledge learned from ImageNet provides essential effects for time series forecasting. This finding underscores the importance of preserving these pre-trained visual features while optimizing for cross-modal transferability during our continual pre-training process.

**Ablation study.** Subsequently, we conduct comprehensive ablation studies to evaluate the contribution of key components in VISIONTS++, with results summarized in Table 4.

- **Vision-model-based Filtering.** Disabling our vision-model-based filtering module results in around 10% performance degradation, confirming its critical role in bridging the data modality gap. Since image pixels are bounded while time series values are unbounded, extreme values in raw time series can disrupt visual representations learned during pre-training.
- **Colorized Multivariate Time Series Conversion.** Removing our colorization strategy (reverting to grayscale image encoding as in VISIONTS) leads to a 7% average MSE degradation. This demonstrates that our RGB-based subfigure encoding effectively transfers the vision model’s multi-object analysis capability to multivariate forecasting. And the colorization scheme also improves cross-variate dependency modeling.
- **Multi-quantile Forecasting.** Reducing our multi-quantile forecasting to a single forecasting head causes over 12% performance decline in both probabilistic and point forecasting. This highlights the effectiveness of our design in unifying deterministic and probabilistic prediction. Unlike methods requiring explicit prior distribution assumptions, we naturally extend MAE’s pixel reconstruction capability to quantile estimation.

**Backbone Scale Analysis.** In Table 5 (with complete results for PF and LTSF in Tables 8 and 9 in Appendix B.3), we present a comparison of three MAE variants: base (112M parameters, consistent with previous experiments), large (330M), and huge (657M). The results show similar performance across model sizes, with not significant differences observed, *e.g.*, the base model performs slightly better on the Monash benchmark while the huge model shows small advantages on the PF benchmark. This near-equivalent performance suggests that when the scale of continual pre-training data and number of training epochs are held constant, increasing model capacity provides limited benefits for the downstream time series forecasting tasks.

However, this finding contrasts with observations from VISIONTS, where larger models were found to be more prone to overfitting to image-specific features, consequently reducing their transferability to time series tasks. This conversely suggests that our continual pre-training framework effectively eliminates these performance disparities, providing strong evidence for its effectiveness in bridging multiple cross-modal gaps. The comparable performance across different model scales demonstrates that our approach successfully adapts visual representations to time series patterns regardless of the backbone’s initial capacity, while maintaining the valuable pre-trained knowledge that enables effective transfer learning.

## 6 Conclusions and Future Work

In this paper, we propose VISIONTS++, a novel time series foundation model built upon the continual pre-training of a vision foundation model on large-scale time series data. To bridge critical inherent gaps between images and time series, we introduce three innovative components, including vision-model-based filtering, colorized multivariate time series conversion, and multi-quantile forecasting. Each of them plays a crucial role in significantly enhancing the model’s forecasting capability.

Extensive experiments on both in-distribution (Monash) and out-of-distribution (LTSF, PF) benchmarks demonstrate that VISIONTS++ achieves state-of-the-art results, significantly outperforming specialized TSF foundation models. These results validate that VISIONTS++ successfully unifies

Table 5: Backbone Analysis on differenten VISIONTS++ sizes.

		base	large	huge
<b>Monash</b>	MAE	<b>0.561</b>	0.566	0.562
<b>PF</b>	MASE	0.677	0.681	<b>0.675</b>
	CRPS	0.515	0.513	<b>0.510</b>
<b>ETTm1</b>	MSE	0.360	0.357	<b>0.356</b>
	MAE	0.372	<b>0.370</b>	<b>0.370</b>
<b>ETTm2</b>	MSE	<b>0.244</b>	0.245	0.246
	MAE	<b>0.298</b>	0.301	0.301
<b>ETTh1</b>	MSE	<b>0.402</b>	0.408	0.407
	MAE	<b>0.416</b>	0.423	0.421
<b>ETTh2</b>	MSE	<b>0.333</b>	0.338	0.336
	MAE	<b>0.370</b>	0.374	0.373
<b>Electricity</b>	MSE	0.184	<b>0.178</b>	0.182
	MAE	0.265	<b>0.261</b>	0.263
<b>Weather</b>	MSE	<b>0.222</b>	0.224	0.226
	MAE	<b>0.241</b>	0.242	0.244

vision and time series modeling, enables effective cross-modal knowledge transfer, and advances the development of vision-based time series foundation models. Importantly, our approach preserves pre-trained visual knowledge while seamlessly adapting to time series patterns, all without requiring any architectural modifications that could disrupt learned representations.

Future directions include exploring larger-scale multi-modal pre-training with bigger vision models and pre-training datasets, extending the foundation model to other time series tasks (*e.g.*, classification, anomaly detection), and investigating dynamic filtering mechanisms for diverse data regimes. Additionally, adapting the method to video-based foundation models could further exploit spatiotemporal correlations, ultimately supporting more powerful universal foundation models that seamlessly integrate visual and time series understanding.

## References

Alon Albalak, Yanai Elazar, Sang Michael Xie, Shayne Longpre, Nathan Lambert, Xinyi Wang, Niklas Muennighoff, Bairu Hou, Liangming Pan, Haewon Jeong, et al. A survey on data selection for language models. [arXiv preprint arXiv:2402.16827](https://arxiv.org/abs/2402.16827), 2024.

Alexander Alexandrov, Konstantinos Benidis, Michael Bohlke-Schneider, Valentin Flunkert, Jan Gasthaus, Tim Januschowski, Danielle C Maddix, Syama Rangapuram, David Salinas, Jasper Schulz, et al. Gluonts: Probabilistic and neural time series modeling in python. [Journal of Machine Learning Research](https://jmlr.org/papers/v21/116.html), 21(116):1–6, 2020.

Abdul Fatir Ansari, Lorenzo Stella, Caner Turkmen, Xiyuan Zhang, Pedro Mercado, Huibin Shen, Oleksandr Shchur, Syama Sundar Rangapuram, Sebastian Pineda Arango, Shubham Kapoor, et al. Chronos: Learning the language of time series. [arXiv preprint arXiv:2403.07815](https://arxiv.org/abs/2403.07815), 2024.

Hangbo Bao, Li Dong, Songhao Piao, and Furu Wei. Beit: Bert pre-training of image transformers. [arXiv preprint arXiv:2106.08254](https://arxiv.org/abs/2106.08254), 2021.

Mouxiang Chen, Lefei Shen, Zhuo Li, Xiaoyun Joy Wang, Jianling Sun, and Chenghao Liu. Visions: Visual masked autoencoders are free-lunch zero-shot time series forecasters. [arXiv preprint arXiv:2408.17253](https://arxiv.org/abs/2408.17253), 2024a.

Ruibo Chen, Yihan Wu, Lichang Chen, Guodong Liu, Qi He, Tianyi Xiong, Chenxi Liu, Junfeng Guo, and Heng Huang. Your vision-language model itself is a strong filter: Towards high-quality instruction tuning with data selection. [arXiv preprint arXiv:2402.12501](https://arxiv.org/abs/2402.12501), 2024b.

Abhimanyu Das, Weihao Kong, Andrew Leach, Shaan Mathur, Rajat Sen, and Rose Yu. Long-term forecasting with tide: Time-series dense encoder. [arXiv preprint arXiv:2304.08424](https://arxiv.org/abs/2304.08424), 2023.

Abhimanyu Das, Weihao Kong, Rajat Sen, and Yichen Zhou. A decoder-only foundation model for time-series forecasting. In [Forty-first International Conference on Machine Learning](https://proceedings.mlr.press/v141/das23a.html), 2024.

Jacob Devlin, Ming-Wei Chang, Kenton Lee, and Kristina Toutanova. BERT: Pre-training of deep bidirectional transformers for language understanding. In [Proceedings of the 2019 Conference of the North American Chapter of the Association for Computational Linguistics: Human Language Technologies, Volume 1 \(Long and Short Papers\)](https://aclanthology.org/N19-1423), pages 4171–4186, Minneapolis, Minnesota, June 2019. Association for Computational Linguistics. doi: 10.18653/v1/N19-1423. URL <https://aclanthology.org/N19-1423>.

Jiaxiang Dong, Haixu Wu, Yuxuan Wang, Yunzhong Qiu, Li Zhang, Jianmin Wang, and Mingsheng Long. Timesiam: A pre-training framework for siamese time-series modeling. [arXiv preprint arXiv:2402.02475](https://arxiv.org/abs/2402.02475), 2024.

Alexey Dosovitskiy, Lucas Beyer, Alexander Kolesnikov, Dirk Weissenborn, Xiaohua Zhai, Thomas Unterthiner, Mostafa Dehghani, Matthias Minderer, Georg Heigold, Sylvain Gelly, Jakob Uszkoreit, and Neil Houlsby. An image is worth 16x16 words: Transformers for image recognition at scale. In [International Conference on Learning Representations](https://proceedings.mlr.press/v131/dosovitskiy21a.html), 2021.

Alex Fang, Albin Madappally Jose, Amit Jain, Ludwig Schmidt, Alexander Toshev, and Vaishaal Shankar. Data filtering networks. [arXiv preprint arXiv:2309.17425](https://arxiv.org/abs/2309.17425), 2023.

Cheng Feng, Long Huang, and Denis Krompass. Only the curve shape matters: Training foundation models for zero-shot multivariate time series forecasting through next curve shape prediction. [arXiv preprint arXiv:2402.07570](#), 2024.

Valentin Flunkert, David Salinas, and Jan Gasthaus. Deepar: Probabilistic forecasting with autoregressive recurrent networks. [International Journal of Forecasting](#), 36, 04 2017. doi: 10.1016/j.ijforecast.2019.07.001.

Fanzhe Fu, Junru Chen, Jing Zhang, Carl Yang, Lvbin Ma, and Yang Yang. Are synthetic time-series data really not as good as real data? [arXiv preprint arXiv:2402.00607](#), 2024.

Jan Gasthaus, Konstantinos Benidis, Yuyang Wang, Syama Sundar Rangapuram, David Salinas, Valentin Flunkert, and Tim Januschowski. Probabilistic forecasting with spline quantile function rns. In [The 22nd international conference on artificial intelligence and statistics](#), pages 1901–1910. PMLR, 2019.

Rakshitha Godahewa, Christoph Bergmeir, Geoffrey I Webb, Rob J Hyndman, and Pablo Montero-Manso. Monash time series forecasting archive. [arXiv preprint arXiv:2105.06643](#), 2021.

Yuan Gong, Yu-An Chung, and James Glass. Ast: Audio spectrogram transformer. [arXiv preprint arXiv:2104.01778](#), 2021.

Mononito Goswami, Konrad Szafer, Arjun Choudhry, Yifu Cai, Shuo Li, and Artur Dubrawski. Moment: A family of open time-series foundation models. [arXiv preprint arXiv:2402.03885](#), 2024.

Sachin Goyal, Pratyush Maini, Zachary C Lipton, Aditi Raghunathan, and J Zico Kolter. Scaling laws for data filtering–data curation cannot be compute agnostic. In [Proceedings of the IEEE/CVF Conference on Computer Vision and Pattern Recognition](#), pages 22702–22711, 2024.

Nate Gruver, Marc Finzi, Shikai Qiu, and Andrew G Wilson. Large language models are zero-shot time series forecasters. [Advances in Neural Information Processing Systems](#), 36:19622–19635, 2023.

Nima Hatami, Yann Gavet, and Johan Debayle. Classification of time-series images using deep convolutional neural networks. In [Tenth international conference on machine vision \(ICMV 2017\)](#), volume 10696, pages 242–249. SPIE, 2018.

Kaiming He, Xinlei Chen, Saining Xie, Yanghao Li, Piotr Dollár, and Ross Girshick. Masked autoencoders are scalable vision learners. In [Proceedings of the IEEE/CVF conference on computer vision and pattern recognition](#), pages 16000–16009, 2022.

Yushan Jiang, Kanghui Ning, Zijie Pan, Xuyang Shen, Jingchao Ni, Wenchao Yu, Anderson Schneider, Haifeng Chen, Yuriy Nevmyvaka, and Dongjin Song. Multi-modal time series analysis: A tutorial and survey. [arXiv preprint arXiv:2503.13709](#), 2025.

Ming Jin, Shiyu Wang, Lintao Ma, Zhixuan Chu, James Y Zhang, Xiaoming Shi, Pin-Yu Chen, Yuxuan Liang, Yuan-Fang Li, Shirui Pan, et al. Time-llm: Time series forecasting by reprogramming large language models. [arXiv preprint arXiv:2310.01728](#), 2023.

Xixi Li, Yanfei Kang, and Feng Li. Forecasting with time series imaging. [Expert Systems with Applications](#), 160:113680, 2020.

Yan Li, Xinjiang Lu, Yaqing Wang, and Dejing Dou. Generative time series forecasting with diffusion, denoise, and disentanglement. [Advances in Neural Information Processing Systems](#), 35: 23009–23022, 2022.

Zekun Li, Shiyang Li, and Xifeng Yan. Time series as images: Vision transformer for irregularly sampled time series. [Advances in Neural Information Processing Systems](#), 36:49187–49204, 2023.

Bryan Lim, Sercan Ö Arik, Nicolas Loeff, and Tomas Pfister. Temporal fusion transformers for interpretable multi-horizon time series forecasting. [International Journal of Forecasting](#), 37(4): 1748–1764, 2021.

Haoxin Liu, Harshavardhan Kamarthi, Zhiyuan Zhao, Shangqing Xu, Shiyu Wang, Qingsong Wen, Tom Hartvigsen, Fei Wang, and B Aditya Prakash. How can time series analysis benefit from multiple modalities? a survey and outlook. [arXiv preprint arXiv:2503.11835](#), 2025a.

Xu Liu, Junfeng Hu, Yuan Li, Shizhe Diao, Yuxuan Liang, Bryan Hooi, and Roger Zimmermann. Unitime: A language-empowered unified model for cross-domain time series forecasting. In [Proceedings of the ACM Web Conference 2024](#), pages 4095–4106, 2024a.

Xu Liu, Juncheng Liu, Gerald Woo, Taha Aksu, Yuxuan Liang, Roger Zimmermann, Chenghao Liu, Silvio Savarese, Caiming Xiong, and Doyen Sahoo. Moirai-moe: Empowering time series foundation models with sparse mixture of experts. [arXiv preprint arXiv:2410.10469](#), 2024b.

Xu Liu, Taha Aksu, Juncheng Liu, Qingsong Wen, Yuxuan Liang, Caiming Xiong, Silvio Savarese, Doyen Sahoo, Junnan Li, and Chenghao Liu. Empowering time series analysis with synthetic data: A survey and outlook in the era of foundation models. [arXiv preprint arXiv:2503.11411](#), 2025b.

Yong Liu, Haoran Zhang, Chenyu Li, Xiangdong Huang, Jianmin Wang, and Mingsheng Long. Timer: Generative pre-trained transformers are large time series models. In [Forty-first International Conference on Machine Learning](#), 2024c.

Ze Liu, Yutong Lin, Yue Cao, Han Hu, Yixuan Wei, Zheng Zhang, Stephen Lin, and Baining Guo. Swin transformer: Hierarchical vision transformer using shifted windows. In [Proceedings of the IEEE/CVF international conference on computer vision](#), pages 10012–10022, 2021.

Ilya Loshchilov and Frank Hutter. Decoupled weight decay regularization. [arXiv preprint arXiv:1711.05101](#), 2017.

Max Marion, Ahmet Üstün, Luiza Pozzobon, Alex Wang, Marzieh Fadaee, and Sara Hooker. When less is more: Investigating data pruning for pretraining llms at scale. [arXiv preprint arXiv:2309.04564](#), 2023.

Casper Meijer and Lydia Y Chen. The rise of diffusion models in time-series forecasting. [arXiv preprint arXiv:2401.03006](#), 2024.

Ilan Naiman, Nimrod Berman, Itai Pemper, Idan Arbit, Gal Fadlon, and Omri Azencot. Utilizing image transforms and diffusion models for generative modeling of short and long time series. [Advances in Neural Information Processing Systems](#), 37:121699–121730, 2024.

Jingchao Ni, Ziming Zhao, ChengAo Shen, Hanghang Tong, Dongjin Song, Wei Cheng, Dongsheng Luo, and Haifeng Chen. Harnessing vision models for time series analysis: A survey. [arXiv preprint arXiv:2502.08869](#), 2025.

Yuqi Nie, Nam H Nguyen, Phanwadee Sinthong, and Jayant Kalagnanam. A time series is worth 64 words: Long-term forecasting with transformers. In [The Eleventh International Conference on Learning Representations](#), 2022.

Youngsuk Park, Danielle Maddix, François-Xavier Aubet, Kelvin Kan, Jan Gasthaus, and Yuyang Wang. Learning quantile functions without quantile crossing for distribution-free time series forecasting. In [International conference on artificial intelligence and statistics](#), pages 8127–8150. PMLR, 2022.

Filip Radenovic, Abhimanyu Dubey, Abhishek Kadian, Todor Mihaylov, Simon Vandenhende, Yash Patel, Yi Wen, Vignesh Ramanathan, and Dhruv Mahajan. Filtering, distillation, and hard negatives for vision-language pre-training. In [Proceedings of the IEEE/CVF conference on computer vision and pattern recognition](#), pages 6967–6977, 2023.

Alec Radford, Jeffrey Wu, Rewon Child, David Luan, Dario Amodei, Ilya Sutskever, et al. Language models are unsupervised multitask learners. [OpenAI blog](#), 1(8):9, 2019.

Artemios-Anargyros Semenoglou, Evangelos Spiliotis, and Vassilios Assimakopoulos. Image-based time series forecasting: A deep convolutional neural network approach. [Neural Networks](#), 157: 39–53, 2023.

ChengAo Shen, Wenchao Yu, Ziming Zhao, Dongjin Song, Wei Cheng, Haifeng Chen, and Jingchao Ni. Multi-modal view enhanced large vision models for long-term time series forecasting. [arXiv preprint arXiv:2505.24003](#), 2025.

Xiaoming Shi, Shiyu Wang, Yuqi Nie, Dianqi Li, Zhou Ye, Qingsong Wen, and Ming Jin. Time-moe: Billion-scale time series foundation models with mixture of experts. [arXiv preprint arXiv:2409.16040](#), 2024.

Srijan Sood, Zhen Zeng, Naftali Cohen, Tucker Balch, and Manuela Veloso. Visual time series forecasting: an image-driven approach. In [Proceedings of the Second ACM International Conference on AI in Finance](#), pages 1–9, 2021.

Hugo Touvron, Matthieu Cord, Matthijs Douze, Francisco Massa, Alexandre Sablayrolles, and Hervé Jégou. Training data-efficient image transformers & distillation through attention. In [International conference on machine learning](#), pages 10347–10357. PMLR, 2021.

Zhiguang Wang and Tim Oates. Imaging time-series to improve classification and imputation. [arXiv preprint arXiv:1506.00327](#), 2015a.

Zhiguang Wang and Tim Oates. Spatially encoding temporal correlations to classify temporal data using convolutional neural networks. [arXiv preprint arXiv:1509.07481](#), 2015b.

Zirui Wang, Zihang Dai, Barnabás Póczos, and Jaime Carbonell. Characterizing and avoiding negative transfer. In [Proceedings of the IEEE/CVF conference on computer vision and pattern recognition](#), pages 11293–11302, 2019.

Ruofeng Wen, Kari Torkkola, Balakrishnan Narayanaswamy, and Dhruv Madeka. A multi-horizon quantile recurrent forecaster. [arXiv preprint arXiv:1711.11053](#), 2017.

Christopher Wimmer and Navid Rekabsaz. Leveraging vision-language models for granular market change prediction. [arXiv preprint arXiv:2301.10166](#), 2023.

Gerald Woo, Chenghao Liu, Akshat Kumar, Caiming Xiong, Silvio Savarese, and Doyen Sahoo. Unified training of universal time series forecasting transformers. In [Forty-first International Conference on Machine Learning](#), 2024.

Haixu Wu, Jiehui Xu, Jianmin Wang, and Mingsheng Long. Autoformer: Decomposition transformers with auto-correlation for long-term series forecasting. [Advances in Neural Information Processing Systems](#), 34:22419–22430, 2021.

Xiongxiao Xu, Yue Zhao, S Yu Philip, and Kai Shu. Beyond numbers: A survey of time series analysis in the era of multimodal llms. [Authorea Preprints](#), 2025.

Luoxiao Yang, Yun Wang, Xinqi Fan, Israel Cohen, Jingdong Chen, Yue Zhao, and Zijun Zhang. Vitime: A visual intelligence-based foundation model for time series forecasting. [arXiv preprint arXiv:2407.07311](#), 2024a.

Yiyuan Yang, Ming Jin, Haomin Wen, Chaoli Zhang, Yuxuan Liang, Lintao Ma, Yi Wang, Chenghao Liu, Bin Yang, Zenglin Xu, et al. A survey on diffusion models for time series and spatio-temporal data. [arXiv preprint arXiv:2404.18886](#), 2024b.

Yunkai Zhang, Yawen Zhang, Ming Zheng, Kezhen Chen, Chongyang Gao, Ruian Ge, Siyuan Teng, Amine Jelloul, Jinmeng Rao, Xiaoyuan Guo, et al. Insight miner: A time series analysis dataset for cross-domain alignment with natural language. In [NeurIPS 2023 AI for Science Workshop](#), 2023.

Haoyi Zhou, Shanghang Zhang, Jieqi Peng, Shuai Zhang, Jianxin Li, Hui Xiong, and Wancai Zhang. Informer: Beyond efficient transformer for long sequence time-series forecasting. In [Proceedings of the AAAI conference on artificial intelligence](#), volume 35, pages 11106–11115, 2021.

Tian Zhou, Ziqing Ma, Qingsong Wen, Xue Wang, Liang Sun, and Rong Jin. Fedformer: Frequency enhanced decomposed transformer for long-term series forecasting. In [International Conference on Machine Learning](#), pages 27268–27286. PMLR, 2022.

Tian Zhou, Peisong Niu, Liang Sun, Rong Jin, et al. One fits all: Power general time series analysis by pretrained lm. [Advances in neural information processing systems](#), 36:43322–43355, 2023.

## Appendix

### A Benchmarks & Baselines

#### A.1 Benchmarks

**Monash Benchmark** Following [Woo et al. \[2024\]](#), we tested 29 Monash datasets [[Godahewa et al., 2021](#)] using GluonTS [[Alexandrov et al., 2020](#)], including M1 Monthly, M3 Monthly, M3 Other, M4 Monthly, M4 Weekly, M4 Daily, M4 Hourly, Tourism Quarterly, Tourism Monthly, CIF 2016, Australian Electricity Demand, Bitcoin, Pedestrian Counts, Vehicle Trips, KDD Cup, Weather, NNS Daily, NNS Weekly, Carparts, FRED-MD, Traffic Hourly, Traffic Weekly, Rideshare, Hospital, COVID Deaths, Temperature Rain, Sunspot, Saugeen River Flow, and US Births. Performance is assessed using Mean Absolute Error (MAE) metric.

**Probabilistic Forecasting Benchmark** The Probabilistic Forecasting (PF) Benchmark [Woo et al. \[2024\]](#) consists of 6 datasets across energy, transport, climate, and sales domains, including Electricity, Solar, Walmart, Weather, Istanbul Traffic, and Turkey Power. Performance is assessed using Continuous Ranked Probability Score (CRPS) and Mean Absolute Scaled Error (MASE) metrics.

**Long-Term TSF Benchmark** We evaluate our model on 6 widely used long-term TSF datasets [[Zhou et al., 2021](#), [Wu et al., 2021](#)], including ETTh1, ETTh2, ETTm1, ETTm2, Electricity, and Weather. Performance is assessed using Mean Squared Error (MSE) and Mean Absolute Error (MAE) metrics.

Table 6: Full results of Monash Time Series Forecasting Benchmark. MAE is reported.

	VisionTS++	VisionTS (z.K.)	LLMTime (z.s.)	Motrai	Motrai	Nave	SUS	Theta	TRATS	ETS	(DHR)-ARIMA	PR	CatBoost	FFNN	DeepAR	N-BEATS	WaveNet	Transformer		
M1 Monthly	5,846.05	1997.69	2892.84	2,082.26	2,082.63	1,983.18	2,707.75	2,759.04	2,066.18	2,317.50	1,905.28	2,008.17	2,088.25	2,025.32	2,022.38	1,860.81	1,820.57	2,184.42	2,723.88	
M3 Monthly	581.68	737.93	877.97	731.41	658.17	664.03	837.14	743.41	623.71	630.59	626.46	654.8	692.37	732	692.48	728.81	648.6	699.3	798.38	
M3 Other	186.13	315.85	300.3	263.54	198.62	202.41	278.43	277.83	215.35	189.4	194.98	193.02	234.43	318.13	240.17	247.56	221.85	245.29	239.24	
M4 Monthly	533.74	666.54	728.27	597.6	592.09	584.36	671.27	625.24	563.58	589.52	582.6	575.36	596.19	611.69	612.52	615.22	578.48	655.51	780.47	
M4 Weekly	200.88	401.22	534.44	230.22	329.32	320.36	290.32	321.22	230.22	230.32	230.22	231.22	230.22	231.22	231.22	231.22	231.22	231.22	231.22	
M4 Daily	172.31	215.63	266.52	189.1	192.66	189.78	180.83	178.27	178.86	176.6	193.26	179.67	181.92	231.36	177.91	299.79	190.44	189.47	201.16	
M4 Hourly	202.99	288.37	576.04	268.04	209.87	197.79	218.06	218.06	368.27	3,358.10	1,310.85	257.39	283.35	385.49	886.02	425.75	393.63	320.54		
Tourism Quarterly	4,056.50	1921.58	10,036.36	1,921.58	1,921.58	1,921.58	1,921.58	1,921.58	1,921.58	1,921.58	1,921.58	1,921.58	1,921.58	1,921.58	1,921.58	9,137.49	9,426.47			
Tourism Quarterly	2,095.71	2560.19	5608.61	3,569.85	2,862.06	2,688.55	5,763.83	5,763.83	5,302.10	1,926.49	9,972.73	8,081.43	10,000.97	9,601.78	10,000.97	8,981.43	9,343.26	8,803.06	9,137.49	
Aus. Elec. Demand	226.31	237.44	760.81	266.57	201.39	177.62	559.6	659.6	665.04	370.74	1,282.99	1,045.92	247.18	247.18	258.76	302.41	213.83	227.46	231.45	
Electricity	1,810.18	2,251.18	1,740.46	1,341.18	1,341.18	1,341.18	7,530.18	7,530.18	1,341.18	1,341.18	1,341.18	1,341.18	1,341.18	1,341.18	1,341.18	1,341.18	1,341.18	1,341.18		
Pedestrian Counts	62.55	52.01	97.77	54.88	54.08	41.66	170.88	170.87	170.94	222.38	216.5	635.16	44.18	43.41	46.41	44.78	66.84	46.46	47.62	
Vehicle Trips	19.98	22.08	31.46	24.48	23.17	21.85	31.42	29.98	30.76	21.21	30.95	30.07	27.24	22.61	22.93	22	28.16	24.15	28.01	
KDD cup	38.89	38.16	42.72	39.81	38.06	32.43	42.13	42.04	42.06	34.88	52.2	34.82	37.1	46.58	49.1	37.98	46.46	46.46		
Weather	1.73	2.16	2.17	1.96	1.8	1.75	2.24	2.24	2.31	2.35	2.45	8.1	7.21	2.09	2.02	2.34	2.29	2.03		
NNS Daily	3.41	3.51	7.1	5.37	4.26	3.77	8.26	6.63	3.8	3.7	3.72	4.41	5.47	4.06	3.94	4.92	3.97	4.16		
NNS Weekly	14.12	14.67	15.76	15.07	16.42	15.3	16.71	15.66	15.3	14.98	15.7	15.38	14.94	15.29	14.69	14.19	14.34	20.54		
Carparts	0.43	0.48	0.44	0.47	0.47	0.45	0.55	0.55	0.56	0.56	0.56	0.56	0.56	0.56	0.56	0.56	0.56	0.56		
FRED-MD	2,347.09	1893.67	2804.64	2,568.48	2,679.29	2,792.55	2,825.67	2,798.22	2,084.42	2,957.11	8,921.94	1,989.97	2,041.42	2,057.11	2,339.57	4,264.36	2,557.68	2,508.40	4,666.04	
Transformer	0.016	0.01	0.01	0.02	0.01	0.03	0.03	0.04	0.04	0.05	0.06	0.06	0.02	0.02	0.03	0.01	0.02	0.01	0.01	
Time Series Weekly	1.07	1.14	1.15	1.14	1.14	1.12	1.13	1.14	1.12	1.17	1.17	1.14	1.11	1.11	1.11	1.12	1.12	1.12		
Rideshare	1.36	5.92	6.28	1.35	1.39	1.29	6.29	7.62	6.45	6.29	3.37	6.3	6.07	6.59	6.28	5.55	2.75	6.29		
Hospital	17.00	19.36	25.68	23	19.4	24.07	21.76	18.54	17.43	17.97	19.6	19.24	19.17	22.08	18.25	20.18	19.35	36.19		
COVID Deaths	151.53	137.51	321.33	124.32	126.11	353.71	353.71	321.32	96.29	85.59	347.98	144.14	201.98	158.81	1,049.48	408.66	1,049.48	408.66		
Temperature Rain	5.17	6.57	5.08	5.08	5.08	5.08	8.18	8.18	8.21	7.59	6.31	5.55	5.57	7.28	7.28	7.28	7.28	7.28		
Sunspot	0.15	2.16	5.07	0.11	0.08	0.13	3.93	4.93	4.93	2.57	4.93	2.57	3.83	2.27	7.97	0.77	14.47	0.17	0.13	
Saugeen River Flow	24.24	30.22	34.84	24.07	24.4	24.76	21.5	21.49	22.26	30.69	25.24	21.28	22.98	23.51	27.92	22.17	28.06			
US Births	411.48	519.94	1374.94	372.51	624.3	476.5	1,152.67	1,192.20	586.93	399	419.73	526.33	574.93	441.7	537.87	424.93	422	504.4	452.87	
Normalized MAE	<b>0.549</b>	0.729	1.041	0.657	0.598	0.576	1.000	1.028	0.927	0.758	0.872	0.898	0.785	0.760	0.741	0.759	0.783	0.749	0.770	

**Baselines** We select multiple representative baselines for comparison, including various time series foundation models as well as other popular TSF baselines covering Transformer-based and MLP-based architectures. These baseline models selected for comparison are briefly described below:

1. **VisionTS** [[Chen et al., 2024a](#)] is a vision-model-based TSF foundation model which utilizes the visual masked autoencoder pre-trained on ImageNet as the backbone model, and reformulate TSF as a patch-level image reconstruction task to complete prediction.
2. **Moirai** [[Woo et al., 2024](#)] is an encoder-based TSF foundation model trained on the Large-scale Open Time Series Archive (LOTSA), with over 231B observations across nine domains. It has three variants: **small**, **base**, and **large**.
3. **Time-MoE** [[Shi et al., 2024](#)] comprises a family of decoder-only transformer models, which leverages a sparse mixture-of-experts (MoE) design by activating only a subset of networks for each prediction to reduce computational load and maintain high model capacity.
4. **Chronos** [[Ansari et al., 2024](#)] tokenizes time series values using scaling and quantization into a fixed vocabulary, and trains T5 family language models (20M to 710M parameters) on these tokenized time series via the cross-entropy loss.
5. **Moment** [[Goswami et al., 2024](#)] family models serve as a building block for diverse time series analysis tasks, are effective out-of-the-box, and are tunable using in-distribution and task-specific data to improve performance.

Table 7: Full results of zero-shot forecasting on the long-term TSF benchmark. **Bold**: the best result.

6. **Timer** [Liu et al., 2024c] is a decoder-based TSF foundation model exhibiting similar characteristics to LLMs, such as flexible context length and autoregressive generation, along with notable few-shot generalization, scalability, and task generality.
7. **TimesFM** [Das et al., 2024] is a decoder-style TSF foundation model, using a large time-series corpus comprising both real-world and synthetic datasets.
8. **LLMTTime** [Gruver et al., 2023] encodes time series data to a text sequence, supporting zero-shot forecasting.
9. **PatchTST** [Nie et al., 2022] uses Transformer encoders with patching and channel independence techniques for improved predictions.
10. **TiDE** [Das et al., 2023] is an MLP-based encoder-decoder TSF model, which enjoys the simplicity and speed of linear models while also being able to handle covariates and non-linear dependencies.
11. **TFT** [Lim et al., 2021] is an attention-based architecture which combines high-performance multi-horizon forecasting with interpretable insights into temporal dynamics.

For the long-term TSF benchmark, we include VISIONTS and other time series foundation models' results from their individual original papers. For the Monash and PF benchmark, we include all results from both Moirai and VISIONTS.

## B Full Experimental Results

## B.1 Full Results for In-distribution Monash Benchmark

Table 6 provides the full breakdown of results for the Monash benchmark, listing results for each dataset in Monash. Based on the table, VISIONTS++ not only obtains SOTA overall normalized MAE results, but also achieves the best results in the vast majority of cases (xx out of 29).

## B.2 Full Results for Out-of-distribution LTSF Benchmark

Table 7 provides the full detailed results for the long-term time series forecasting experiments, listing results for each prediction length. From the results, we can see that VISIONTS++ achieves the best results in most cases (xx out of 62), outperforming VISIONTS (xx out of 62), Time-MoE(large) (xx out of 62), and all other models.

Table 8: Full results on PF benchmark of the backbone analysis on different VISIONTS++ sizes.

Dataset	Method	base	large	huge
<b>Electricity</b>	CRPS	0.042	0.042	<b>0.041</b>
	MASE	0.631	0.633	<b>0.628</b>
<b>Solar</b>	CRPS	<b>0.353</b>	0.357	0.355
	MASE	<b>1.155</b>	1.162	1.161
<b>Walmart</b>	CRPS	0.064	<b>0.062</b>	<b>0.062</b>
	MASE	<b>0.689</b>	<b>0.689</b>	0.691
<b>Weather</b>	CRPS	0.038	<b>0.037</b>	0.039
	MASE	<b>0.447</b>	0.451	<b>0.447</b>
<b>Istanbul Traffic</b>	CRPS	0.115	0.112	<b>0.106</b>
	MASE	0.616	0.617	<b>0.592</b>
<b>Turkey Power</b>	CRPS	<b>0.036</b>	0.038	0.038
	MASE	<b>0.737</b>	0.746	0.749
<b>Average</b>	CRPS	0.677	0.681	<b>0.675</b>
	MASE	<b>0.515</b>	0.513	<b>0.510</b>
<b>1st Count</b>		6	3	8

Table 9: Full results on LTSF benchmark of the backbone analysis on different VISIONTS++ sizes.

Method	base		large		huge		
	Metric	MSE	MAE	MSE	MAE	MSE	MAE
<b>ETTm1</b>	96	0.316	0.343	<b>0.314</b>	<b>0.342</b>	<b>0.314</b>	0.343
	192	0.347	0.362	<b>0.344</b>	<b>0.360</b>	<b>0.344</b>	<b>0.360</b>
	336	0.368	0.379	0.367	0.376	<b>0.363</b>	<b>0.375</b>
	720	0.408	0.405	0.403	<b>0.401</b>	<b>0.402</b>	<b>0.401</b>
	avg	0.360	0.372	0.357	<b>0.370</b>	<b>0.356</b>	<b>0.370</b>
<b>ETTm2</b>	96	<b>0.169</b>	<b>0.248</b>	0.172	0.250	0.173	0.253
	192	<b>0.216</b>	0.279	0.218	0.283	0.217	<b>0.278</b>
	336	<b>0.260</b>	<b>0.308</b>	0.261	0.312	0.263	0.310
	720	<b>0.330</b>	<b>0.358</b>	0.330	0.360	0.332	0.362
	avg	<b>0.244</b>	<b>0.298</b>	0.245	0.301	0.246	0.301
<b>ETTh1</b>	96	<b>0.369</b>	<b>0.392</b>	0.371	0.395	0.374	0.396
	192	<b>0.399</b>	<b>0.412</b>	0.403	0.414	0.401	0.413
	336	<b>0.415</b>	<b>0.421</b>	0.417	0.427	0.415	0.423
	720	<b>0.424</b>	<b>0.437</b>	0.442	0.456	0.438	0.451
	avg	<b>0.402</b>	<b>0.416</b>	0.408	0.423	0.407	0.421
<b>ETTh2</b>	96	0.277	0.326	<b>0.273</b>	<b>0.324</b>	<b>0.273</b>	0.325
	192	<b>0.333</b>	<b>0.362</b>	0.336	0.367	0.337	0.365
	336	<b>0.350</b>	<b>0.384</b>	0.362	0.389	0.354	0.386
	720	<b>0.370</b>	<b>0.409</b>	0.380	0.415	0.381	0.416
	avg	<b>0.333</b>	<b>0.370</b>	0.338	0.374	0.336	0.373
<b>Electricity</b>	96	0.152	0.237	<b>0.148</b>	<b>0.233</b>	0.150	0.234
	192	0.168	0.252	<b>0.163</b>	<b>0.248</b>	0.166	<b>0.248</b>
	336	0.186	0.269	<b>0.180</b>	<b>0.265</b>	0.187	0.267
	720	0.228	0.303	<b>0.219</b>	<b>0.296</b>	0.226	0.303
	avg	0.184	0.265	<b>0.178</b>	<b>0.261</b>	0.182	0.263
<b>Weather</b>	96	<b>0.145</b>	0.179	<b>0.145</b>	<b>0.178</b>	0.146	0.180
	192	<b>0.187</b>	<b>0.219</b>	0.189	0.220	0.190	0.221
	336	<b>0.240</b>	<b>0.258</b>	0.242	0.259	0.245	0.262
	720	<b>0.317</b>	<b>0.308</b>	0.318	0.310	0.321	0.312
	avg	<b>0.222</b>	<b>0.241</b>	0.224	0.242	0.226	0.244
<b>Average</b>		<b>0.291</b>	<b>0.327</b>	0.292	0.328	0.292	0.329
<b>1st Count</b>		38	20	12			

### B.3 Full Results for Backbone Scale Analysis

#### B.3.1 PF Benchmark

Table 8 reports the full detailed results on the PF benchmark for the backbone analysis of Table 5.

#### B.3.2 LTSF Benchmark

Table 9 reports the full detailed results on the LTSF benchmark for the backbone analysis of Table 5.

## C Visualization

In this section, we visualize the multivariate time series predictions of VISIONTS++ in the zero-shot setting, including its input and reconstructed images. We also visualize its predictions, with MSE and MAE metrics for comparison. These samples are presented in Figure 4 and Figure 5.

These examples show the superior forecasting performance of VISIONTS++ over VISIONTS after conducting the continual pre-training, effectively addressing the modality gaps between images and time series.

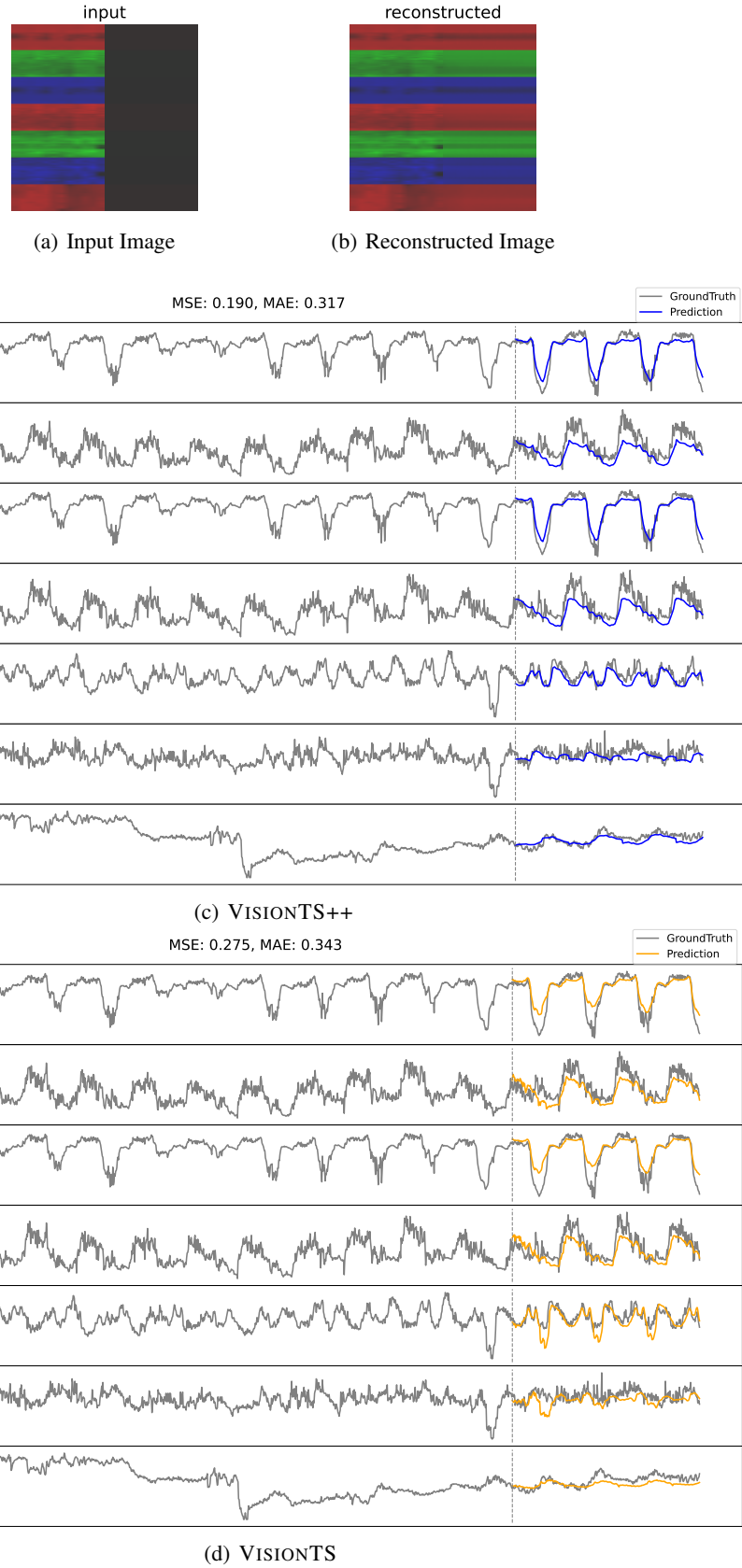
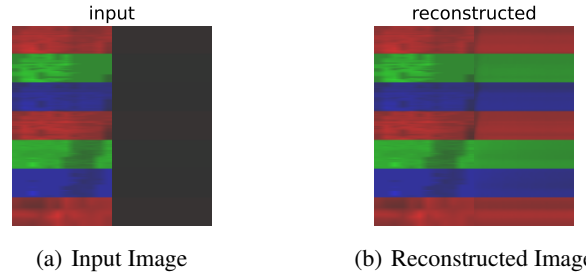
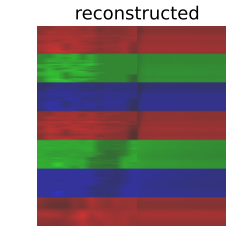


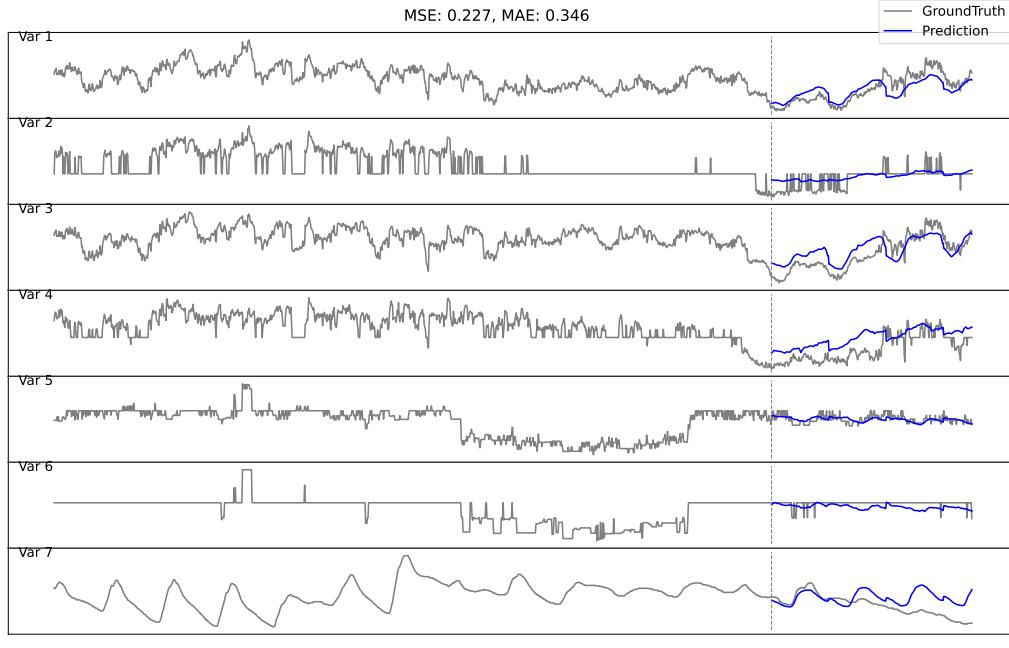
Figure 4: Forecasting visualization on a sample from ETTm1. (a-b) Input/Output images of VISIONTS++. (c-d) Prediction comparison between VISIONTS++ and VISIONTS.



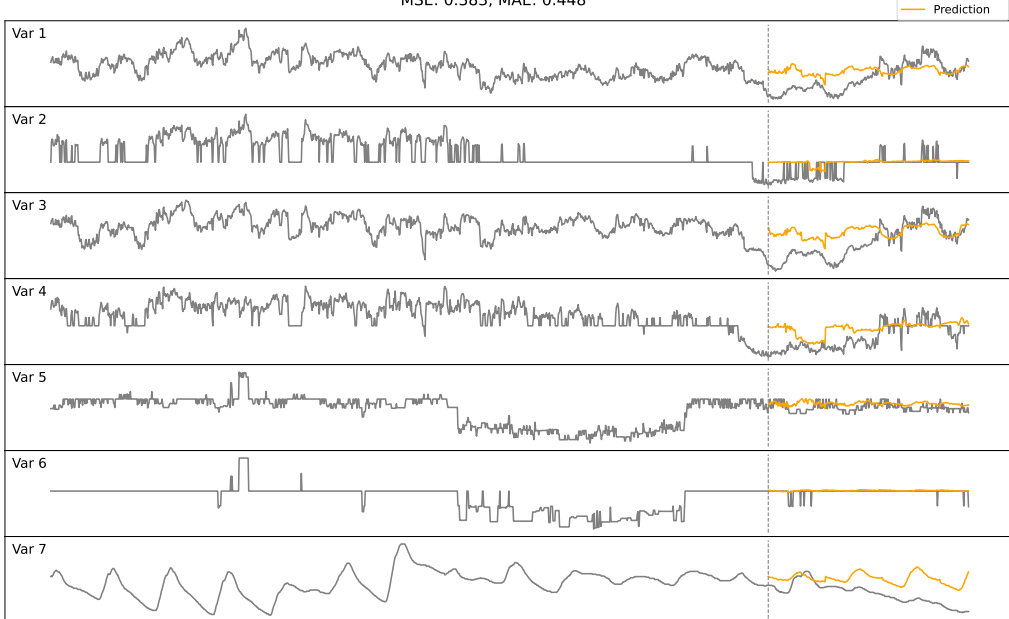
(a) Input Image



(b) Reconstructed Image



MSE: 0.383, MAE: 0.448



(d) VISIONTS

Figure 5: Forecasting visualization on a sample from ETTm2. (a-b) Input/reconstructed images of VISIONTS++. (c-d) Prediction comparison between VISIONTS++ and VISIONTS.